Capacitive Sensor Design Utilizing Conformal Mapping Methods

N. Eidenberger, B. G. Zagar
Institute for Measurement Technology
Johannes Kepler University, Altenberger Strasse 69,
4040 Linz, Austria
Emails: norbert.eidenberger@jku.at, bernhard.zagar@jku.at

Submitted: Dec. 28, 2011 ***Accepted: Jan. 31, 2012*** ***Published: Mar. 1, 2012***

Abstract-In this work we demonstrate the advantages of conformal mapping methods for the design of capacitive sensor setups. If the setups are modeled appropriately, the respective Laplace equations can be solved utilizing conformal mapping methods. These methods yield the equations describing the electric field of the sensor setups. The field equations contain the distinct geometric properties of the sensor setups. An in depth analysis of these equations permits the optimization of the sensor setups with respect to their sensitivities. This approach also facilitates the application of efficient signal processing methods. In addition, we propose a method which expands the application range of conformal maps produced by the Schwarz-Christoffel transform. This method permits the analysis of more complex sensor setups.

Index terms*: Conformal mapping, Schwarz-Christoffel transform, Joukowski tranform, capacitance sensor, electric field, blade geometry, edge geometry, sensitivity analysis.

I. INTRODUCTION

An important aspect during the development of a sensor consists in considering the relevant properties of the quantity which is to be measured. As soon as these properties have been identified, the sensor setup can be designed appropriately. The quality of the developed sensor setup can be determined utilizing different approaches, e.g. by finite element methods (FEM), physical modeling, or test measurements with sensor prototypes. Sensor prototypes can be costly and are therefore rarely utilized. FEM often provide useful results for complex setups when analytical methods cannot be utilized. Nevertheless, analytical methods have advantages, e.g. when the influence of varying geometries on the measurement result is of interest.

In this work we analyze two different capacitive sensor setups, one for measuring the angle of an edge, one for measuring the quality of a blade. For each setup the Laplace equation is solved utilizing conformal mapping methods. Conformal maps provide an uncommon yet elegant way of constructing the field equations for certain types of problems which occur in diverse technical fields. Some current applications of conformal mapping methods are presented e.g. in [1], [2], [3], [4], and [5].

Conformal mapping methods map a simple reference setup to complex electrode setups. The respective conformal mapping functions connect the known electric field distribution of the simple setup to the complex one. This approach yields the analytic expression for the electric field of the complex setup which describes the electric field of the complex electrode setup in terms of the position and the geometric parameters. The main disadvantage of conformal mapping methods consists in their restriction to two dimensional problems. However, many real world problems can be approximated by two dimensional models.

The basics of conformal mapping are given in [6] and [7]. A particularly useful method for obtaining conformal maps, the Schwarz-Christoffel Transform (SCT), is presented in detail in [8]. The SCT has been developed to map structures which form polygons, which is often the case in technical applications. In order to obtain a conformal mapping function through the SCT its parameters need to be computed. If the polygon consists of more than three corners, the SCT parameters cannot be computed analytically which constitutes the so-called SCT parameter problem [7]. We propose an approximation method based on a series expansion which permits the computation of an approximate analytic solution for the SCT parameter problem for polygons consisting of four corners or more. Thus, this method permits an in depth analysis of such sensor setups with respect to their geometric parameters.

This article is organized in three parts. The first part presents a method for constructing conformal maps for capacitive sensor setups containing an air gap by combining different methods. In addition the connection between conformal mapping functions and the corresponding electric field equations is presented. The second part illustrates the construction of conformal maps and the corresponding field equations for two example setups. For the analysis of the edge measurement setup an exact solution is obtained, while for the blade measurement setup the proposed approximation method is employed. The third part illustrates the advantage of the obtained analytical field equations by performing sensitivity analyses with respect to the geometric parameters of the sensor setups.

II. CONFORMAL MAPPING

In this section a method for the construction of a conformal mapping function for sensor setups consisting of polygonal electrodes separated by an air gap is developed. In general it is difficult to obtain a conformal mapping function except for simple problems. There exists no generally applicable method for the construction of conformal maps, even though the Riemann mapping theorem guarantees the existence of conformal maps [6]. Instead there exist various methods for constructing conformal maps for different types of problems. The most commonly utilized methods are presented in [6], and [9], along with the fundamentals of conformal mapping theory.

Figure 1 illustrates the idea of conformal mapping. The ideal plate capacitor is positioned in the *w*-plane where lines parallel to the u-axis represent equipotentials, and lines parallel to the *v*-axis represent the lines of electrical force. The coordinates are interpreted as components of a complex number $w = u + j\,v$ which are mapped to the z-plane with $z = x + j\,y$ via a complex valued function $z = f(w)$. The function $z = f(w)$ represents the desired conformal map which leads to the solution of the Laplace equation.

The proposed method combines three different conformal transforms in order to obtain a conformal mapping function for polygonal electrodes separated by an air gap:

1) Schwarz-Christoffel transform (SCT),
2) Joukowski transform,
3) Polar transform.

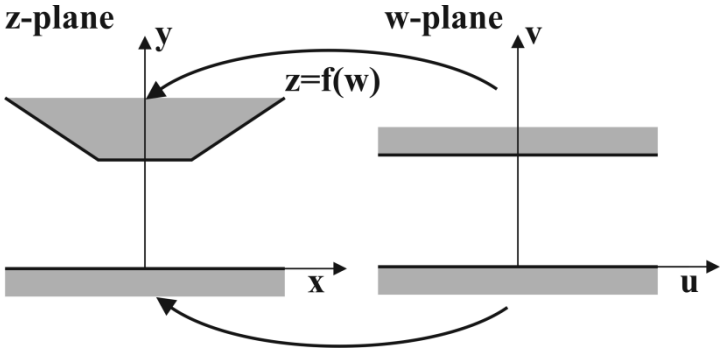

Figure 1. The idea of conformal mapping. The region between the electrodes of the infinite plate capacitor in the *w*-plane is mapped conformally to the region between the polygon and the plane in the *z*-plane by a mapping function *f(z)*.

Each transform models a different property of a sensor setup. Linking these transforms together yields a function which conformally maps an ideal infinite plate capacitor to the measurement setup. The ideal infinite plate capacitor is utilized as the reference setup due to its simple field structure.

a. Schwarz-Christoffel Transform

The SCT has been developed to map structures which are bounded by polygons. There are two variants of the SCT. One maps the upper half of a complex plane to the interior of polygons and the real axis to the polygon boundary. The other maps the unit circle to the polygons and the circle boundary to the polygon boundary. In this paper the former SCT variant is utilized which maps the upper half of the *w*-plane (image plane) to the polygons in the complex *z*-plane (object plane). The general equation for this SCT variant is defined by (1).

$$z = A \int \prod_{i=1}^{n} (w - w_i)^{\frac{\alpha_i}{\pi} - 1} dw + B \tag{1}$$

In (1) *z* and *w* represent the complex variables of the *z*- and *w*-planes respectively, the α_i represent the interior angles of the polygon corners, the w_i represent the so called prevertices, which denote the position of the images of the edges of the polygons in the image plane *w*. The prevertices and their corresponding angles define the general shape of the polygon whereas the parameters *A* and *B* define scaling, rotation, and translation of the polygon. In order to be able to compute the unknown parameters *A*, *B* and w_i of the SCT it is necessary to construct an appropriate model of the problem. This can be achieved, e.g. by taking advantage of the symmetry of the original problem and using the method of images. The SCT parameters are then computed by comparing the positions of the polygon corners in the *z*- and *w*-plane.

b. Joukowski Transform

The Joukowski transform introduces gaps into closed contours. Alternatively, it can also be utilized to model the potential of a closed contour with two corners. Its general form is defined by (2).

$$z = \frac{d}{2}\left(w + \frac{1}{w}\right) \tag{2}$$

In (2) *z* and *w* represent the complex variables of the *z*- and *w*-planes, and the parameter *d* represents the gap length. The gap is centered at the origin of the *w*-plane and can be positioned by adding a complex valued constant to (2). The Joukowski transform is utilized to introduce an air gap into the mapping function.

c. Polar Transform

The polar transform introduces two different potentials into the mapping function. Its general form is defined by (3).

$$z = e^{w} \tag{3}$$

In (3) *z* and *w* again represent the complex variables of the *z*- and *w*-planes.

These three transforms represent the elements which comprise the conformal mapping function which maps the ideal plate capacitor to a sensor setup. The transforms are actually applied in reverse order. First, the conformal mapping function applies the polar transform to the ideal plate capacitor. This maps the capacitor electrodes in the *w*-plane to the real axis of an intermediate complex plane where the electrodes touch at the origin and form an uninterrupted line. Next, the Joukowski transform maps the line to another intermediate complex plane where the electrodes are separated by a gap centred at the origin. Finally, the SCT maps the broken line from the real axis to the electrodes of the sensor setup model in the *z*-plane.

Several intermediate complex planes are utilized during the construction of the mapping. Different coordinate sets describe the different intermediate complex planes. In order to simplify the notation during the construction of the conformal mapping function *z=f(w)*, the variable *w* is repeatedly substituted for the right sides of (3) and (2) instead of introducing different complex variables. However, the illustrations of the intermediate planes are labelled utilizing different variables in order to distinguish them properly.

Equation (4) connects the field equation describing the electric field to the conformal mapping function.

$$E(z) = -\operatorname{grad}\phi(z) = -\operatorname{grad}\psi(w)\cdot\left(\overline{f'(w)}\right)^{-1} \tag{4}$$

In (11) *E(z)* and $\phi(z)$ respectively represent the electric field and the potential distribution in the *z*-plane, $\psi(w)$ represents the potential distribution in the *w*-plane, and *f(w)* represents the conformal mapping function. The derivation of this relation can be found in [6] or [10].

The potential distribution $\psi(w)$ depends on the choice for the reference setup. In this case the ideal infinite plate capacitor is utilized, for which $\psi(w)$ is well known. If the potential of the electrode at $v=0$ is set to zero and the potential of the electrode at $v=d$ is set to *V* then (5) defines $\psi(w)$ where *d* represents the distance between the electrodes of the ideal plate capacitor.

$$\psi(w) = j\frac{V}{d}v \tag{5}$$

The illustration in figure 1 implies that $\psi(w)=\psi(u,v)$. Therefore, lines of constant *u* represent the lines of electric force, and lines of constant *v* represent equipotentials. These lines are mapped to curves in the *z*-plane.

III. APPLICATION EXAMPLES

In this section two measurement setups are analyzed utilizing conformal mapping methods. The conformal mapping function for the edge measurement setup is obtained by utilizing the standard methods whereas for the blade measurement setup the proposed approximation method needs to be employed.

a. Edge measurement setup

The first example consists of the capacitive measurement setup illustrated in figure 2. The setup consists of an edge which is positioned at a height *h* above a sensor array. The edge angle is defined as 2α. Conformal mapping will be utilized to obtain the field equation for the electric field between the edge and the sensor array in terms of the geometric parameters of the measurement setup. The mapping function will be constructed according the approach presented in chapter II. The presented approach improves and extends previous work which has been presented in [11].

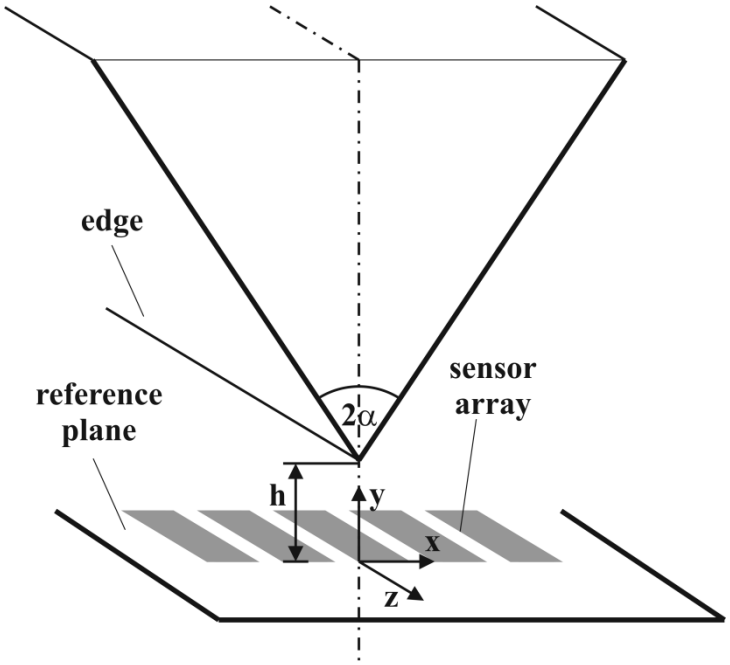

Figure 2. Illustration of the edge measurement setup.

a.i Schwarz-Christoffel transform

In order to be able to construct the SCT an appropriate model of the measurement setup is required. Instead of utilizing a 2D version of the setup model illustrated in figure 2 a different but electrically equivalent model is created. The new model is constructed by taking advantage of the symmetry in the proposed setup and applying the method of images. Figure 3 illustrates the final model including its geometric parameters h and α_i.

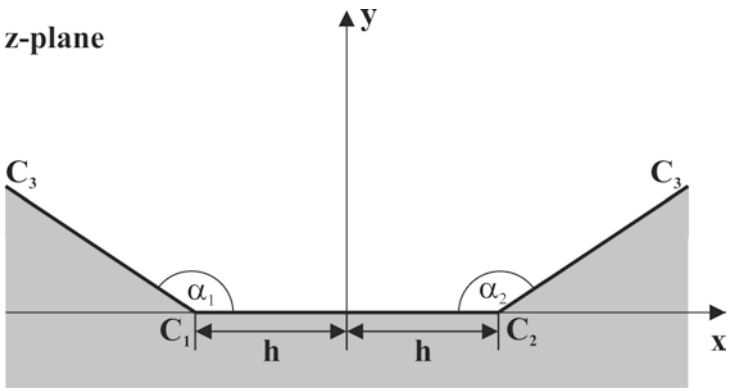

Figure 3. Illustration of the appropriate symmetric model of the measurement setup which is utilized to construct the SCT.

The model illustrated in figure 3 contains only three corners, therefore the SCT parameters can be computed analytically. The SCT maps the auxiliary t_1-plane illustrated in figure 4 to the model in figure 3. The base form of the SCT for the modeled setup is obtained by insert-

ing the prevertices and the corresponding angles into (1). The position of the prevertices is selected with w_1=-1, w_2=1, and w_3=∞. For the prevertice at infinity no angle needs to be defined [6]. The remaining angles are $\alpha_1=\alpha_2=\alpha\pi$. Inserting these parameters into (1) yields (6).

$$z = A \int (w^2 - 1)^{-\alpha}\, dw + B \tag{6}$$

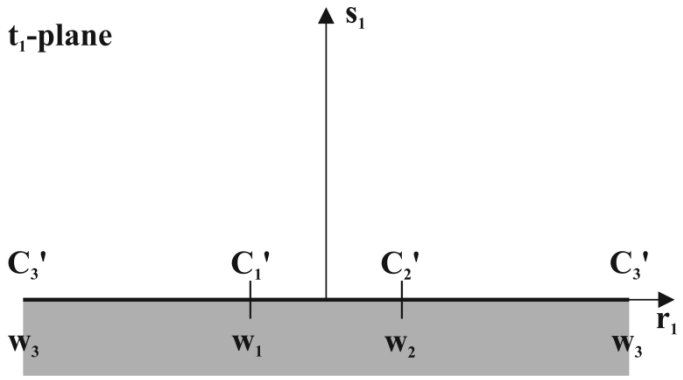

Figure 4. The auxiliary plane for the SCT illustrates the position w_i of the prevertices.

In the next step, the remaining SCT parameters *A* and *B* need to be determined. Computing the integral in (6) results in a function which contains singularities at *w=1* and *w=-1*. These singularities prohibit the computation of the SCT parameters. In order to avoid these singularities (6) is multiplied by the constant factor $(-1)^{-\alpha}$ which yields (7). This factor is absorbed by the generic parameter *A* and does not influence the final SCT.

$$z = A \int (1 - w^2)^{-\alpha}\, dw + B \tag{7}$$

The evaluation of the integral in (7) yields (8) which contains the hypergeometric function ${}_2F_1(a,b;c;x)$, a so-called special function. Details about special functions can be found in [12] or at [13].

$$z = A w\, {}_2F_1\left(\frac{1}{2}, \alpha; \frac{3}{2}; w^2\right) + B \tag{8}$$

The remaining unknown parameters A and B are now computed by comparing the positions of the corners in the different planes illustrated in figure 3 and 4 utilizing (8). The solution for the system of equations is given in (9) and (10).

$$A = \frac{2h\Gamma\left(\frac{3}{2} - \alpha\right)}{\sqrt{\pi}\Gamma(1 - \alpha)} \tag{9}$$

$$B = 0 \tag{10}$$

The solutions for the SCT parameters only depend on the geometric parameters of the measurement setup. This is important for the subsequent analysis of the setup. Parameter *A* also

contains the Euler gamma function $\Gamma(x)$. Inserting A and B into (8) yields the SCT (11) which maps the upper half of a complex plane to the contour in figure 3.

$$z = \frac{2hw\Gamma\left(\frac{3}{2}-\alpha\right)}{\sqrt{\pi}\Gamma(1-\alpha)}\,{}_2F_1\left(\frac{1}{2},\alpha;\frac{3}{2};w^2\right) \tag{11}$$

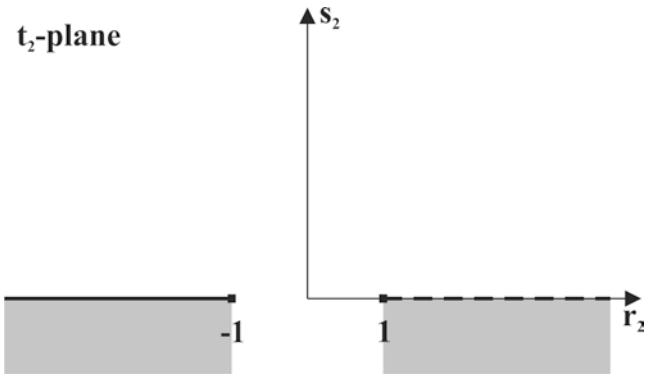

Figure 5. The auxiliary plane for the Joukowski transform illustrates the position of the introduced air gap.

a.ii Joukowski transform

Following the construction of the SCT, the Joukowski transform introduces the air gap to the mapping function by replacing the complex variable w in (11) by the right hand side of (2) which yields (12). Figure 5 illustrates the position of the air gap in the auxiliary t_2-plane.

$$z = \frac{h\left(w+\frac{1}{w}\right)\Gamma\left(\frac{3}{2}-\alpha\right)}{\sqrt{\pi}\Gamma(1-\alpha)}\,{}_2F_1\left(\frac{1}{2},\alpha;\frac{3}{2};\frac{1}{4}\left(w+\frac{1}{w}\right)^2\right) \tag{12}$$

a.iii Polar transform

The last step in the construction of the conformal mapping function consists in introducing the polar transform to (12). Replacing w in (12) by the right hand side of (3) yields the desired mapping function (13) which conformally maps the ideal plate capacitor to the edge measurement setup. The function (13) depends on the position as well as on the geometric parameters of the measurement setup. The domain of definition consists of $u=[0,\infty[;\ v=[-\pi/2,0]$ which maps only one half of the measurement setup. Due to the setup symmetry the result just needs to by mirrored about the y-axis in order to obtain the result for the whole measurement setup.

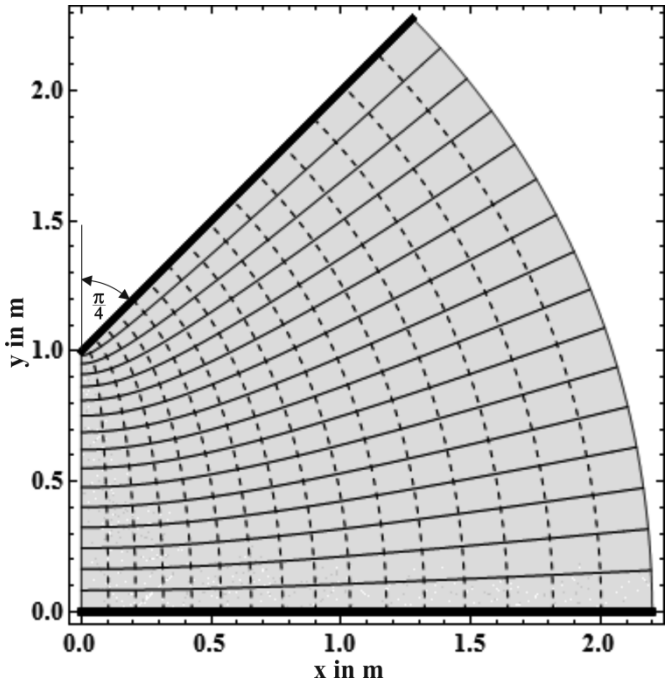

Figure 6. Visualization of (13) for an example setup with *h=1* m and $\alpha=\pi/4$ rad. Solid lines represent equipotential lines, dashed lines represent lines of electrical force.

$$z = \frac{2jh\Gamma\left(\frac{3}{2}-\alpha\right)}{\sqrt{\pi}\Gamma(1-\alpha)}\cosh(w)\,{}_2F_1\left(\frac{1}{2},\alpha;\frac{3}{2};\cosh^2(w)\right) \tag{13}$$

The mapping function (13) is visualized in figure 6 for an example geometry. There the bold solid lines represent the electrodes, the solid lines represent equipotentials, and the dashed lines represent the lines of electrical force.

a.iv Field equation

According to relation (4) the field equation depends on the conformal mapping function (13) and the gradient of the potential distribution grad$(\psi(w))$ of the reference setup. According to (5) and considering the domain of definition for (13), grad$(\psi(w))=-2jV/\pi$. Inserting this relation and the conformal mapping function (13) into (5) yields the field equation (14), which describes the electric field between the electrodes of the measurement setup where *V* represents the potential of the edge and the potential of the sensor array is set to zero.

$$E(z) = -\frac{V\Gamma(1-\alpha)\,\mathrm{csch}\left(\overline{w}\right)\left(-\sinh^2\left(\overline{w}\right)\right)^{\alpha}}{\sqrt{\pi}h\Gamma\left(\frac{3}{2}-\alpha\right)} \tag{14}$$

Figure 7 illustrates the electric field in the measurement setup. The field equation (14) can be utilized to analyse the measurement setup.

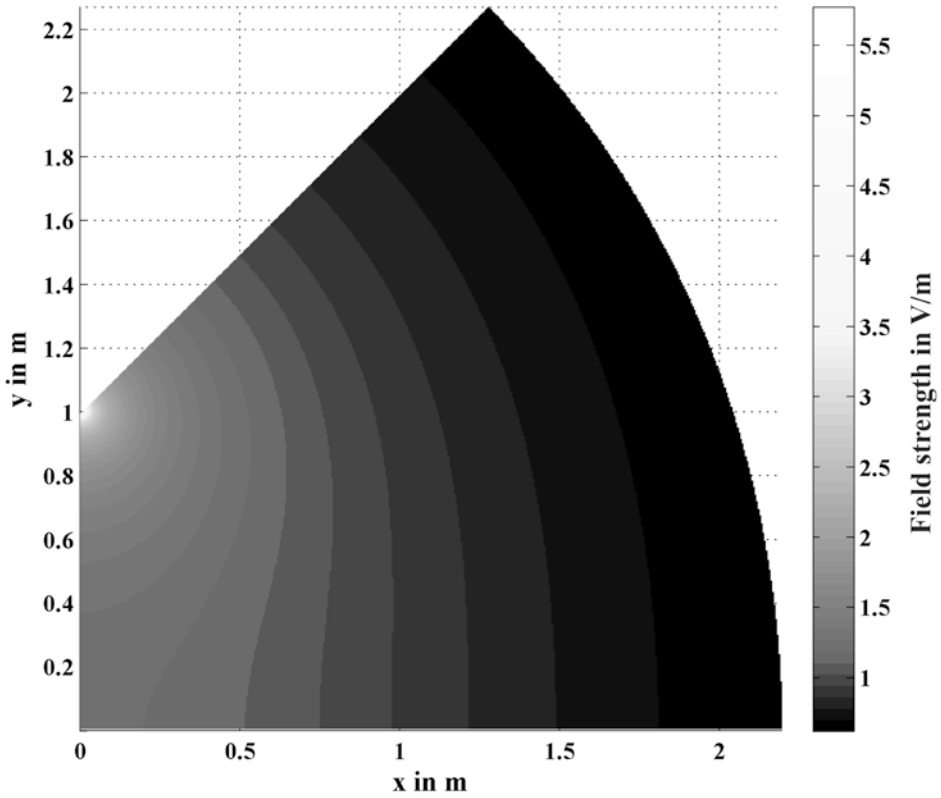

Figure 7. Visualization of (14) for an example setup with $h=1$ m and $a=\pi/4$ rad.

b. Blade Measurement Setup

The second example consists of the capacitive measurement setup illustrated in figure 8. The setup consists of a blade which is positioned at a height h above a sensor array. The blade is defined by two parameters, which consist of the blade angle α and the height of the blade b. Again conformal mapping will be utilized to obtain the field equation describing this measurement setup. Because of the larger number of electrode corners, an approximation method needs to be employed in order to be able to construct the SCT. The presented approach improves and extends previous work which has been presented in [14].

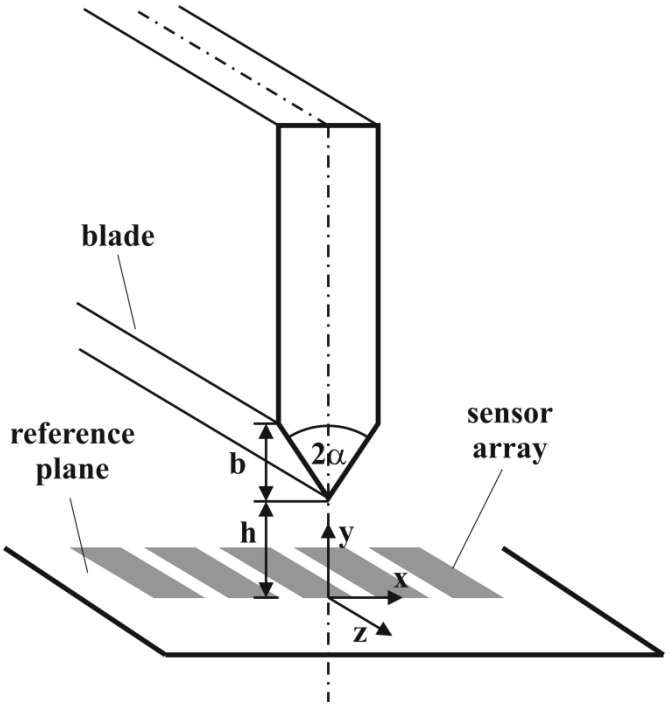

Figure 8. Illustration of the blade measurement setup.

b.i Schwarz-Christoffel transform

In order to be able to construct the SCT an appropriate model of the measurement setup is required. Instead of utilizing a 2D version of the setup model illustrated in figure 8 a different but electrically equivalent model is created. The new model is constructed by taking advantage of the symmetry in the proposed setup and applying the method of images. Figure 9 illustrates the final model including its geometric parameters *h*, *b*, and α_i.

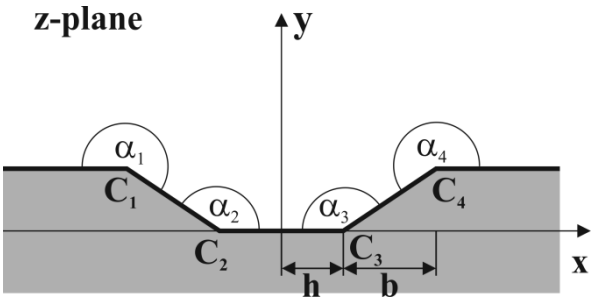

Figure 9. Illustration of the appropriate symmetric model of the measurement setup which is utilized to construct the SCT.

The model illustrated in figure 9 contains four corners. This means that the SCT parameters cannot be computed analytically. The SCT maps the auxiliary t_1-plane illustrated in figure 10 to the model in figure 9. The base form of the SCT for the modeled setup is obtained by in-

serting the prevertices and the corresponding angles into (1). The position of the prevertices is selected with $w_1=-k$, $w_2=-1$, $w_3=1$, and $w_4=k$. The corresponding angles are $\alpha_1=\pi+\alpha\,\pi$, $\alpha_2=\pi-\alpha$, $\alpha_3=\pi-\alpha$, and $\alpha_4=\pi+\alpha$. Inserting these parameters into (1) yields (15).

$$z = A\int\left(\frac{w^2-k^2}{w^2-1}\right)^{\alpha} dw + B \tag{15}$$

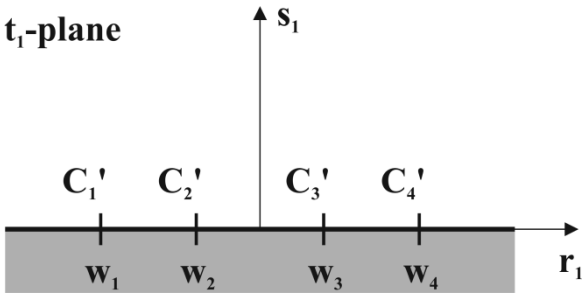

Figure 10. The auxiliary plane for the SCT illustrates the position w_i of the prevertices.

Computing the integral in (15) results in (16) which contains the Appell function $F_1(\alpha;\beta,\beta';\gamma';x,y)$. Details about this special function can be found in [12] or at [15]. Next, the remaining SCT parameters need to be determined.

$$z = Awk^{2\alpha}F_1\left(\frac{1}{2};\alpha,-\alpha;\frac{3}{2};w^2,\frac{w^2}{k^2}\right)+B \tag{16}$$

The SCT parameters A, B, and k are computed by comparing the positions of the corners in the different planes which are illustrated in figure 9 and 10. This yields three equations with three unknown parameters. In order to solve this system of equations the inverse of the Appell function is required. Unfortunately, no inverse of the Appell function exists. This means that the solution cannot be computed analytically. It is of course possible to use numerical methods to solve the system of equations. However, this would render it impossible to formulate a mapping function which explicitly contains the geometric parameters. In order to solve the problem analytically a linear approximation (17) of the Appell function (16) is utilized.

$$z = Ak^{2\alpha}w \tag{17}$$

Utilizing the approximation permits the computation of the SCT parameters. The results are given in (18), (19) and (20).

$$A = h\left(1+\frac{b}{h}\right)^{-2\alpha} \tag{18}$$

$$B = 0 \tag{19}$$

$$k = 1+\frac{b}{h} \tag{20}$$

Inserting the SCT parameters yields the result for the SCT (21) which maps between the upper half plane in figure 10 and the contour in figure 9. Due to the linearization an approximation error has been introduced to the conformal mapping function.

$$z = hwF_1\left(\frac{1}{2}; \alpha, -\alpha; \frac{3}{2}; w^2, \frac{h^2 w^2}{(b+h)^2}\right) \tag{21}$$

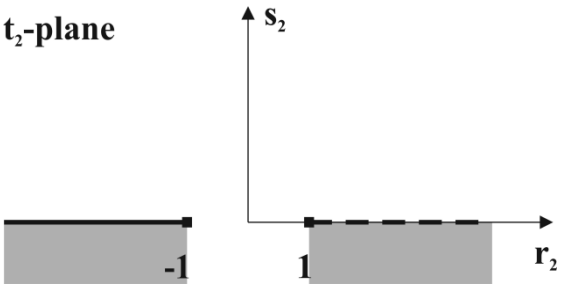

Figure 11. The auxiliary plane for the Joukowski transform illustrates the position of the introduced air gap.

b.ii Joukowski transform

Following the construction of the SCT, the Joukowski transform introduces the air gap to the mapping function by replacing the complex variable *w* in (21) by the right hand side of (2) which yields (22). Figure 11 illustrates the position of the air gap in the auxiliary t_2-plane.

$$z = \frac{1}{2}h\left(w + \frac{1}{w}\right) F_1\left(\frac{1}{2}; \alpha, -\alpha; \frac{3}{2}; \frac{1}{4}\left(w + \frac{1}{w}\right)^2, \frac{h^2\left(w + \frac{1}{w}\right)^2}{4(b+h)^2}\right) \tag{22}$$

b.iii Polar transform

The last step in the construction of the conformal mapping function consists in introducing the polar transform to (22). Replacing *w* in (22) by the right hand side of (3) yields the desired mapping function (23) which maps the ideal plate capacitor conformally to the blade measurement setup. The function depends on the position as well as on the geometric parameters of the measurement setup. The domain of definition consists of $u=[-\infty,0[$; $v=[\pi/2,\pi]$ which maps only one half of the measurement setup. Due to the setup symmetry the result just needs to by mirrored about the *y*-axis in order to obtain the result for the whole measurement setup.

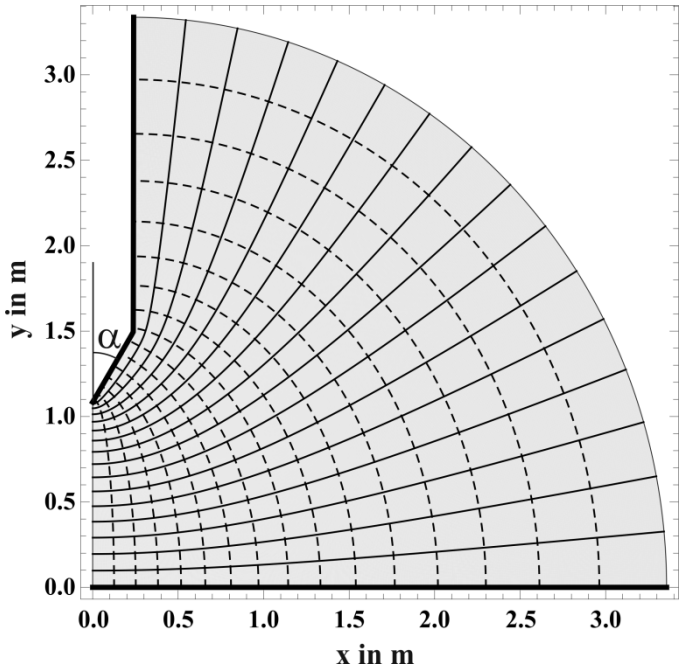

Figure 12. Visualization of (23) for an example setup with *h=1* m, *b=0.5* m and $\alpha=\pi/3$ rad. Solid lines represent equipotential lines, dashed lines represent lines of electrical force.

$$z = -jh\cosh(w)F_1\left(\frac{1}{2};\alpha,-\alpha;\frac{3}{2};\cosh^2(w),\frac{h^2\cosh^2(w)}{(b+h)^2}\right) \tag{23}$$

The mapping function (23) is visualized in figure 12 for an example geometry. There the bold solid lines represent the electrodes, the solid lines represent equipotentials, and the dashed lines represent the lines of electrical force. The effect of the approximation error on the mapping result is visible at the corners of the blade contour. The positions of the blade tip and the blade corner deviate from the desired position. Note that the blade angle is mapped correctly because the approximation only influences the mapping of lengths.

b.iv Field equation

Considering the domain of definition for (23) the gradient of the potential distribution grad$(\psi(w))=2jV/\pi$. Inserting this relation and the conformal mapping function (23) into (5) yields the field equation (24), which describes the electric field between the electrodes of the measurement setup where *V* represents the potential of the edge and the potential of the sensor array is assumed to be zero.

$$E(z) = \frac{2V}{\pi h}\operatorname{csch}(\overline{w})\left(-\sinh^2(\overline{w})\right)^{\alpha}\left(1-\frac{h^2\cosh^2(\overline{w})}{(b+h)^2}\right)^{-\alpha} \tag{24}$$

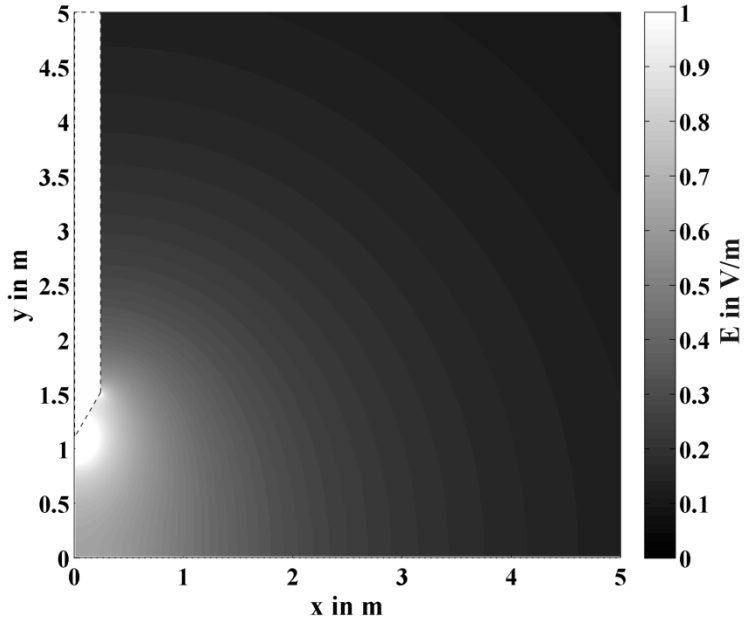

Figure 13. Visualization of (24) for an example setup with $h=1$ m, $b=0.5$ m and $\alpha=\pi/3$ rad.

Figure 13 illustrates the electric field in the measurement setup which contains an approximation error. However, a verification of (24) by FEM showed that although the field equation (24) produces a result for a version of the measurement setup with warped lengths, the field is nevertheless correct for the warped setup. This means that the electric field for the desired measurement setup can be obtained by simply adjusting the lengths of the measurement setup accordingly prior to the mapping. Thus, the field equation (24) can be utilized to analyse the measurement setup.

IV. SETUP ANALYSES

The field equations permit simple and fast analyses of the measurement setups. The sensitivities of the different setups with respect to variations of the setup geometry can easily be computed. This simplifies the determination of the placement and the optimal shape of the single sensor elements of the sensor array. In this section the sensitivities for the measurement setups are computed and illustrated by evaluating the resulting equations at the position of the respective sensor array.

a. Sensitivity of the Edge Measurement Setup

The sensitivities at the position of the sensor array are computed by deriving (14) with respect to the geometric parameters. This approach yields equations which contain the edge angle α and the air gap length *h* and can be evaluated at arbitrary coordinates *w*.

The sensitivity of the measurement setup with respect to the air gap length *h* is given by (25). Figure 14 illustrates the sensitivity at the position of the sensor array for an example setup geometry. As expected, the sensitivity is inverse proportional to variations of *h* and the maximum sensitivity occurs at the point which is closest to the edge.

$$\frac{\partial E(z)}{\partial h} = \frac{V\Gamma(1-\alpha)\,\mathrm{csch}\,(\overline{w})\left(-\sinh^2(\overline{w})\right)^{\alpha}}{\sqrt{\pi}h^2\Gamma\left(\frac{3}{2}-\alpha\right)} \tag{25}$$

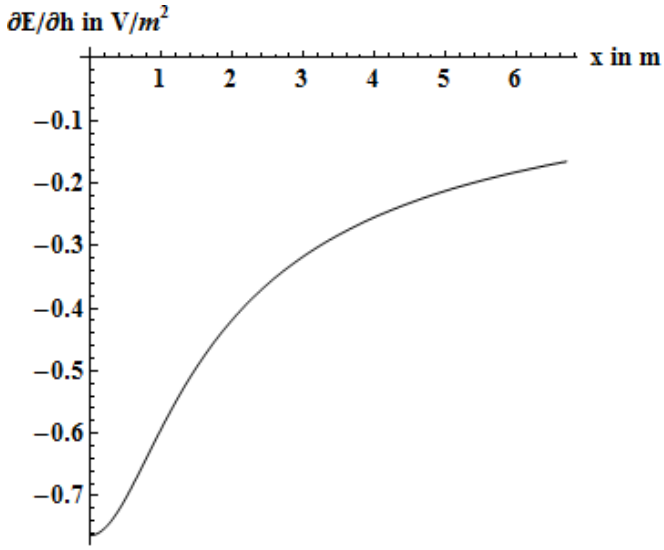

Figure 14. Visualization the sensitivity with respect to the air gap length *h* along the *x*-axis of the edge measurement setup for *h=1* m, *α=π/4* rad and *V=1* V.

The sensitivity of the measurement setup with respect to the edge angle α is given by (26) where H_n represents the nth harmonic number. Figure 15 illustrates the sensitivity at the position of the sensor array for an example setup geometry. It shows that the sensitivity is inverse proportional to variations of α and the sensitivity peaks at some distance from the point of symmetry.

$$\frac{\partial E(z)}{\partial \alpha} = -\frac{V\Gamma(1-\alpha)\,\mathrm{csch}\,(\overline{w})\left(-\sinh^2(\overline{w})\right)^{\alpha}\left(\log\left(-\sinh^2(\overline{w})\right)+H_{\frac{1}{2}-\alpha}-H_{-\alpha}\right)}{\sqrt{\pi}h\Gamma\left(\frac{3}{2}-\alpha\right)} \tag{26}$$

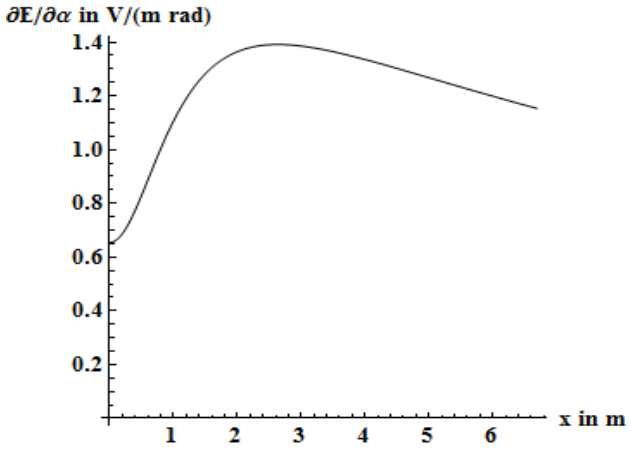

Figure 15. Visualization the sensitivity with respect to the edge angle α along the *x*-axis of the edge measurement setup for *h=1* m, *α=π/4* rad and *V=1* V.

b. Sensitivity of the Blade Measurement Setup

The sensitivities at the position of the sensor array are computed by deriving (24) with respect to the geometric parameters. This approach yields equations which contain the blade angle α, the blade height *b*, and the air gap length *h* and can be evaluated at arbitrary coordinates *w*. The sensitivity of the measurement setup with respect to the air gap length *h* is given by (27). Figure 16 illustrates the sensitivity at the position of the sensor array for an example setup. As expected, the sensitivity is inverse proportional to variations in *h*, and the maximum sensitivity occurs at the point which is closest to the blade tip.

$$\frac{\partial E(z)}{\partial h} = -\frac{2V\,\mathrm{csch}\,(\overline{w})\left(-\sinh^2(\overline{w})\right)^{\alpha}\left(1-\frac{h^2\cosh^2(\overline{w})}{(b+h)^2}\right)^{-\alpha}\left(h^2\cosh^2(\overline{w})\,(2b\alpha+b+h)-(b+h)^3\right)}{\pi h^2(b+h)\left(h^2\cosh^2(\overline{w})-(b+h)^2\right)} \tag{27}$$

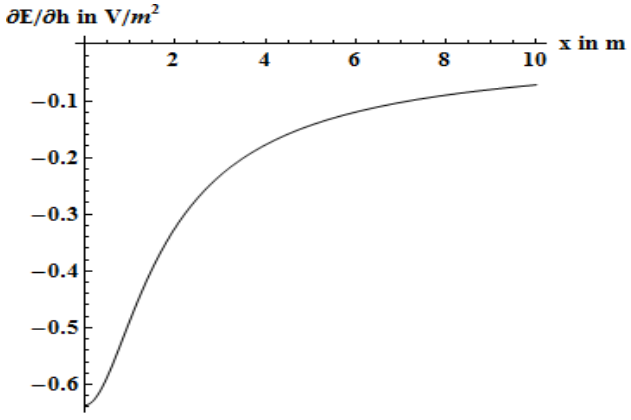

Figure 16. Visualization the sensitivity with respect to the air gap length *h* along the *x*-axis of the edge measurement setup for *h=1* m, *b=0.5* m, *α=π/6* rad and *V=1* V.

The sensitivity of the measurement setup with respect to the blade angle α is given by (28). Figure 17 illustrates the sensitivity at the position of the sensor array for an example setup. It shows that the sensitivity is proportional to variations of α and the sensitivity peaks at some distance from the point of symmetry.

$$\frac{\partial E(z)}{\partial \alpha} = -\frac{2V\,\mathrm{csch}\,(\overline{w})\left(-\sinh^2(\overline{w})\right)^{\alpha}\left(1-\frac{h^2\cosh^2(\overline{w})}{(b+h)^2}\right)^{-\alpha}\left(\log\left(1-\frac{h^2\cosh^2(\overline{w})}{(b+h)^2}\right)-\log\left(-\sinh^2(\overline{w})\right)\right)}{\pi h} \tag{28}$$

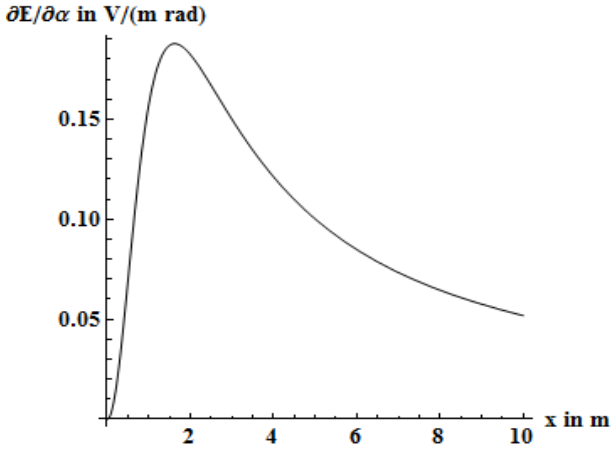

Figure 17. Visualization the sensitivity with respect to the blade angle α along the *x*-axis of the edge measurement setup for $h=1$ m, $b=0.5$ m, $\alpha=\pi/6$ rad and $V=1$ V.

The sensitivity of the measurement setup with respect to the blade height *b* is given by (29). Figure 18 illustrates the sensitivity at the position of the sensor array for an example setup. It shows that the sensitivity is proportional to variations of *b* and the sensitivity peaks at some distance from the point of symmetry.

$$\frac{\partial E(z)}{\partial b} = -\frac{4hV\alpha\cosh(\overline{w})\coth(\overline{w})\left(-\sinh^2(\overline{w})\right)^{\alpha}\left(1-\frac{h^2\cosh^2(\overline{w})}{(b+h)^2}\right)^{-\alpha-1}}{\pi(b+h)^3} \tag{29}$$

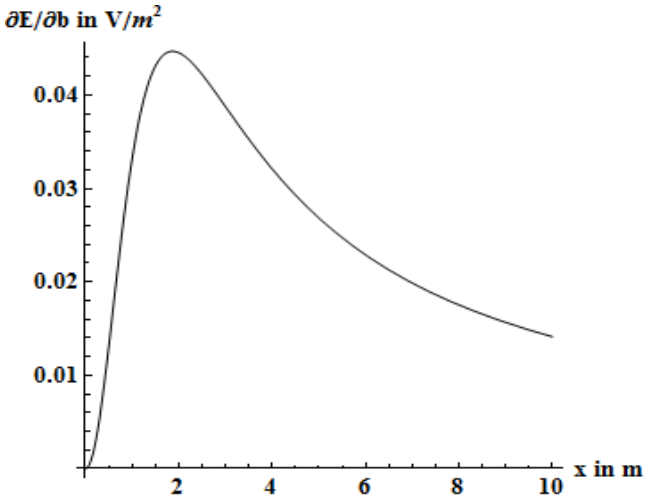

Figure 18. Visualization the sensitivity with respect to the blade height *b* along the *x*-axis of the edge measurement setup for $h=1$ m, $b=0.5$ m, $\alpha=\pi/6$ rad and $V=1$ V.

V. CONCLUSION

In this paper the application of conformal mapping methods for constructing field equations for two different capacitive measurement setups has been presented. An approximation method for solving the SCT parameter problem has been introduced, which permits the analysis of more complex setups. The obtained field equations vastly simplify all further analyses concerning sensor design, measurement setup analysis, and sensor signal processing. In particular, this permits solving the inverse problem which consists in reconstructing the three dimensional shape of the objects which cause the two dimensional electric field distribution measured by the sensor array.

ACKNOWLEDGEMENT

The authors gratefully acknowledge the partial financial support for the work presented in this paper by the Austrian Research Promotion Agency and the Austrian COMET program supporting the Austrian Center of Competence in Mechatronics (ACCM).

REFERENCES

[1] T. Sun, N. G. Green, and H. Morgan, “Electric field analysis using schwarz-christoffel mapping,” Journal of Physics: Conference Series, vol. 142, no. 1, p. 012029, 2008.

[2] E. Starschich, A. Muetze, and K. Hameyer, “An alternative approach to analytic force computation in permanent-magnet machines,” Magnetics, IEEE Transactions on, vol. 46, no. 4, pp. 986–995, Apr. 2010.

[3] A. Webster, “Magnetohydrodynamic stability at a separatrix. II. Determination by new conformal map technique,” Physics of Plasmas, vol. 16, no. 8, p. 082503 (10 pp.), Aug. 2009.

[4] P. W. Cattaneo, “Capacitances in micro-strip detectors: A conformal mapping approach,” Solid-State Electronics, vol. 54, no. 3, pp. 252–258, 2010.

[5] Y.-H. Su, J.-S. Yang, and C.-R. Chang, “Schwarz-Christoffel transformation for cladding conducting lines,” Magnetics, IEEE Transactions on, vol. 45, no. 10, pp. 3800–3803, Oct. 2009.

[6] P. Henrici, Applied and Computational Complex Analysis, ser. Pure & Applied Mathematics, A Wiley Interscience Series of Texts, Monographs & Tracts. John Wiley & Sons, 1974, vol. 1.

[7] P. Henrici, Applied and Computational Complex Analysis, ser. Pure & Applied Mathematics, A Wiley Interscience Series of Texts, Monographs & Tracts. John Wiley & Sons, 1986, vol. 3.

[8] T. A. Driscoll and L. N. Trefethen, Schwarz–Christoffel Mapping, ser. Cambridge Monographs on Applied and Computational Mathematics, P. Ciarlet, A. Iserles, R. Kohn, and M. Wright, Eds. Cambridge University Press, 2002.

[9] R. Schinzinger and A. Laura, Conformal Mapping: Methods and Applications. Elsevier, 1991.

[10] W. Smythe, Static and Dynamic Electricity, 3rd ed. Hemisphere Publ., 1989.

[11] N. Eidenberger and B. G. Zagar, „Capacitive Sensor Setup for the Measurement and Tracking of Edge Angles“, Proc. *ICARA 2011*, pp. 361-365, New Zealand, December 6-8, 2011.

[12] E. T. Whittaker and G. N. Watson, A Course of Modern Analysis, 4th ed. Cambridge University Press, 1973.

[13] E. W. Weisstein. (2011, Jul.) Hypergeometric function. From MathWorld–A Wolfram Web Resource. [Online]. Available: http://mathworld.wolfram.com/HypergeometricFunction.html

[14] N. Eidenberger and B. G. Zagar, „Sensitivity of Capacitance Sensors for Quality Control in Blade Production“, Proc. *ICST 2011*, pp. 433-437, New Zealand, Nov. 28- Dec.1, 2011.

[15] E. W. Weisstein. (2011, Jul.) Appell Hypergeometric Function. From MathWorld–A Wolfram Web Resource. [Online]. Available: http://mathworld.wolfram.com/AppellHypergeometricFunction.html